Slow fusion pore expansion creates a unique reaction chamber for co-packaged cargo

Kevin P. Bohannon,[1]* Mary A. Bittner,[1]* Daniel A. Lawrence,[2,3] Daniel Axelrod,[1,4,5] and Ronald W. Holz[1]

[1]Department of Pharmacology, [2]Department of Internal Medicine, [3]Department of Molecular and Integrative Physiology, [4]Department of Physics, and [5]LSA Biophysics, University of Michigan, Ann Arbor, MI

A lumenal secretory granule protein, tissue plasminogen activator (tPA), greatly slows fusion pore dilation and thereby slows its own discharge. We investigated another outcome of the long-lived narrow fusion pore: the creation of a nanoscale chemical reaction chamber for granule contents in which the pH is suddenly neutralized upon fusion. Bovine adrenal chromaffin cells endogenously express both tPA and its primary protein inhibitor, plasminogen activator inhibitor 1 (PAI). We found by immunocytochemistry that tPA and PAI are co-packaged in the same secretory granule. It is known that PAI irreversibly and covalently inactivates tPA at neutral pH. We demonstrate with zymography that the acidic granule lumen protects tPA from inactivation by PAI. Immunocytochemistry, total internal reflection fluorescence (TIRF) microscopy, and polarized TIRF microscopy demonstrated that co-packaged PAI and tPA remain together in granules for many seconds in the nanoscale reaction chamber, more than enough time to inhibit tPA and create a new secreted protein species.

INTRODUCTION

Upon fusion of the secretory granule with the plasma membrane, lumenal constituents are discharged at very different rates. This is explained in some cases by molecular size. For example, a low molecular weight neurotransmitter such as epinephrine is usually discharged in fewer than 100 ms, whereas co-stored proteins can be released over many seconds. Specific proteins can be discharged at widely different rates independently of cell type. GFP-tagged neuropeptide Y (NPY) and tissue plasminogen activator (tPA) have contrasting behaviors. NPY usually discharges within several hundred milliseconds of fusion, whereas tPA discharges after many seconds in primary chromaffin cells (Perrais et al., 2004), PC12 cells (Taraska et al., 2003), and insulin-secreting cells (Tsuboi et al., 2004). This large difference is unlikely to reflect simply a difference in the molecular weights of the proteins (tPA-GFP, ∼100 kD; NPY-GFP, ∼40 kD). Indeed, there is another explanation. By measuring the orientation of a fluorescent probe within the plasma membrane with polarized total internal reflection fluorescence (pTIRF) microscopy, we found that more than two-thirds of the fusion events of tPA-cerulean–containing granules maintain curvature for greater than 10 s (Weiss et al., 2014a). The maintained curvature reflects a narrow fusion pore. This conclusion is consistent with the finding using a fluorescent cytosolic probe that tPA-containing granules maintain long-lived, volume-enclosing structures on the surface of PC12 cells (Taraska et al., 2003). Such events are uncommon upon fusion of fluorescent-labeled NPY-containing granules. Indeed, pTIRF microscopy (Anantharam et al., 2010a; Weiss et al., 2014a) and real-time imaging of invaginations on the cell surface (Chiang et al., 2014) reveal that curvature changes and volume-filling omega figures resulting from fusion of NPY-containing granules have a much shorter duration, often no longer than several hundred milliseconds. tPA initiates an autocrine/paracrine pathway through its proteolytic enzymatic activity that locally regulates subsequent exocytosis within the adrenal medulla (Parmer et al., 1997, 2000). Thus, the slow postfusion discharge of tPA at the cell surface likely influences the kinetics of the pathway.

The ability of tPA to almost freeze the fusion pore may have effects in addition to slowing its own release. Our experiments explore the notion that the inhibition of fusion pore expansion creates a novel compartment on the cell surface in which undiluted lumenal proteins are suddenly exposed to a pH shift from 5.5 to 7.4. We explore the implications of this concept in the context of the biochemistry of tPA.

tPA is best known as a circulating serine protease that converts plasminogen into plasmin, which in turn breaks down fibrin clots by proteolysis. The activity of tPA in the plasma is regulated by plasminogen activator inhibitor 1 (PAI), a protein that acts as a suicide substrate to covalently inhibit the proteolytic activity of

*K.P. Bohannon and M.A. Bittner contributed equally to this paper.
Correspondence to Kevin P. Bohannon: kevbo@umich.edu

Abbreviations used: DBH, dopamine-β-hydroxylase; NPY, neuropeptide Y; PAI, plasminogen activator inhibitor 1; pHl, pHluorin; PSS, physiological saline solution; pTIRF, polarized TIRF; TIRF, total internal reflection fluorescence; tPA, tissue plasminogen activator.

The Rockefeller University Press
J. Gen. Physiol. 2017 Vol. 149 No. 10 921–934
https://doi.org/10.1085/jgp.201711842

tPA. These proteins are clinically important. Recombinant tPA is used intravenously to treat stroke (Fugate and Rabinstein, 2014), and dysregulation of tPA and PAI secretion is associated with thrombophilia (Sartori et al., 2003), hyperfibrinolysis (Ladenvall et al., 2000), obesity (Dietrich et al., 2016), and angiogenesis. tPA is expressed in many tissues including vascular endothelial cells (Loscalzo and Braunwald, 1988), adrenal chromaffin cells (Parmer et al., 1997), posterior pituitary nerve terminals (Miyata et al., 2005), and central nervous system (hypothalamic) neurons (Salles and Strickland, 2002).

PAI and tPA are expressed in the adrenal medulla. Both colocalize with large dense-core catecholamine-containing chromaffin granules in sucrose density gradients (Parmer et al., 1997; Jiang et al., 2011). Both are co-secreted with catecholamine upon stimulation with a nicotinic agonist or elevated K^+. We had previously found by immunocytochemistry that tPA is readily detected in chromaffin granules in ∼20% of primary cultured chromaffin cells (Weiss et al., 2014b). In the present study, we show that PAI is expressed in a much larger fraction of chromaffin cells and that in tPA-expressing cells, PAI is colocalized in granules with tPA. We demonstrate that the low intragranular pH (pH 5.5) protects tPA from inactivation by co-stored PAI and investigate PAI discharge and the effects of PAI on both fusion pore dynamics and the discharge rate of coexpressed fluorescently labeled tPA. The results lead us to propose the formation of a nanoscale reaction chamber created by the fused granule and the long-lived narrow fusion pore that prevents rapid release of proteins but permits a sudden increase in lumenal pH. This compartment likely regulates the amount of enzymatically active tPA released extracellularly and creates a new molecular entity, the tPA/PAI complex, which may itself have a physiological function.

MATERIALS AND METHODS

Molecular biology

Constructs used to express human tPA, tPA-pHluorin (tPA-pHl), tPA-S513A, tPA-S513A-pHl, PAI, and PAI-pHl were created using synthetic gBlocks (Integrated DNA Technologies) as described in Supplemental Methods. For consensus sequences, accession no. NM_000930.4 was used for human tPA and accession no. NM_000602.4 for human PAI. NPY-pHl was a gift of W. Almers (Vollum Institute, Oregon Health and Science University, Portland, OR).

Chromaffin cell transfection

Primary bovine adrenal medullary chromaffin cells were isolated as previously described (Wick et al., 1993), plated on 35-mm glass-bottom dishes (refractive index 1.51; World Precision Instruments), treated with poly-D-lysine, and layered with bovine collagen. Chromaffin cells were transfected with the Neon Transfection System (Invitrogen). Cells were electroporated in Invitrogen's proprietary Solution R or in a homemade resuspension buffer (250 mM sucrose and 1 mM $MgCl_2$ in Dulbecco's PBS; Brees and Fransen, 2014). 10^6 cells and up to 10 µg DNA in 100 µl total resuspension buffer were electroporated with pulse settings of 1,100 mV and 40 ms. In cases where an unlabeled construct was transfected along with a fluorescently labeled construct, the unlabeled construct was added in excess, at a ratio of 2:1.

Immunocytochemistry

Chromaffin cells were stained and analyzed as described in detail in the figure legends. Images were acquired on an Olympus Fluoview 500 confocal microscope with a 60× 1.42-NA oil objective. An argon 488-nm laser with a 505- to 525-nm bandpass filter, a HeNe green 543-nm laser with a 560- to 600-nm bandpass filter, and a HeNe red (633-nm) laser with a longpass filter were used. To minimize spillover, images with different excitations were acquired sequentially. Within an experiment, initial settings were adjusted so that the brightest pixels for each color were unsaturated, and these settings were maintained throughout. Images were analyzed with ImageJ (Schneider et al., 2012), and statistics were analyzed with GraphPad Prism 6.

Antibodies and reagents

Antibodies were as follows: rabbit anti–mouse tPA, sheep anti–human tPA (Molecular Innovations); unlabeled and Alexa Fluor 488–labeled goat anti–rabbit Fab fragments (Jackson ImmunoResearch); rabbit anti–human PAI (Abcam); Alexa Fluor–labeled secondary antibodies (Life Technologies; Molecular Probes).

Microscopy

Live cell experiments were conducted on an inverted Olympus IX70 microscope with a 1.49-NA objective and a specialized pTIRF excitation scheme as previously described (Weiss et al., 2014a). A 488-nm laser (Coherent OBIS or Melles Griot 543-AP-01) was used to visualize pHluorin, and a 561-nm laser polarized into P- and S-polarizations (Coherent OBIS) was used to visualize the carbocyanine dye, 1,1′-dioctadecyl-3,3,3′,3′-tetramethylindodicarbocyanine, 4-chlorobenzenesulfonate salt (DiD). The filter cube contained a dichroic mirror/emission filter combination: ZT488/561rpc and ZET488/561m for NPY-pHl/DiD or tPA-pHl/DiD (Chroma Technology). The aligned excitation beams were focused and positioned near the periphery of the back focal plane of a 60× 1.49-NA, oil immersion objective (Olympus) so that the laser beam was incident on the coverslip at ∼70° from the normal giving a decay constant for the evanescent field of ∼100 nm. The galva-

nometer mirrors were computer controlled through a DAQ board, NI PCIE-6351 (National Instruments) and a custom LabVIEW program.

The system was programmed to step through a sequence of three shutter openings (one at a time for each beam), repeating the cycle without additional delay using a through-the-lens (TTL) triggering system (sequence frequency, 8 Hz). Emission images (with the 1.5× internal magnifying lens in the emission path) were acquired by a cooled EM-CCD camera (iXon, 512 × 512 pixels; Andor Technology). Camera control and serial image acquisition was managed by Solis (Andor Technology). Sequential NPY-pHl or tPA-pHl and DiD emission images (the latter excited sequentially by S- and P-polarized 561-nm laser beams and denoted *S* and *P*, respectively) were captured. Normalized *P/S* ratios and *P*+2*S* sums were calculated pixel by pixel for each image, and the transformations were aligned to the pHluorin images using custom software written in IDL.

For pHl secretion experiments without DiD, images were acquired at a rate of 36 Hz on an iXon EMCCD camera (Andor Technologies). For pTIRF secretion experiments, shuttering was used to sequentially image pHl, P-polarized DiD, and S-polarized DiD at a rate of 8.5 Hz. All experiments were performed in a 34°C room to approximate physiological temperatures.

Perfusion

All experiments were performed 3–5 d posttransfection in a room heated to 34 ± 1°C. Previous experiments from the laboratory were performed at 27°C (Weiss et al., 2014a,b); the higher temperature was used to better approximate the normal physiological temperature of the granules. Individual cells were perfused through a pipette (100-µm inner diameter) using positive pressure from a computer-controlled perfusion system DAD-6VM (ALA Scientific Instruments). Cells were maintained in a calcium physiological saline solution (CaPSS) plus glucose (145 mM NaCl, 5.6 mM KCl, 2.2 mM $CaCl_2$, 0.5 mM $MgCl_2$, 5.6 mM glucose, and 15 mM Hepes, pH 7.4). Other solutions used during perfusion were elevated potassium PSS (KPSS; 95 mM NaCl, 56 mM KCl, 2.2 mM $CaCl_2$, 0.5 mM $MgCl_2$, 5.6 mM glucose, and 15 mM Hepes, pH 7.4) and low pH MES buffer (145 mM NaCl, 5.6 mM KCl, 2.2 mM $CaCl_2$, 0.5 mM $MgCl_2$, 5.6 mM glucose, and 15 mM MES, pH 5.5). Generally, cells were treated according to the following schedule during perfusion: 3 s CaPSS, 3 s MES, 3 s CaPSS, 45 s KPSS, 5 s MES, and 10 s CaPSS. Before pTIRF imaging experiments, a saturated solution of DiD in ethanol was added to cells at a concentration of 1:500 and immediately rinsed three times with PSS.

Analysis of event duration

pHluorin-labeled protein discharge was measured over time for a small region of interest (~0.7-µm diameter) centered on the event using Time Series Analyzer V2.0 plugin in ImageJ. Time-varying local backgrounds were determined by capturing the intensity of a neighboring region of interest without a fusion event. They were subtracted frame by frame from the intensities of the discharge events. The local background subtraction was necessary because of increases in background intensity caused by protein diffusion from nearby events.

The duration of discharge of pHluorin-labeled proteins was determined with a custom program that largely eliminated subjectivity of the analysis and greatly facilitated the interpretation of the results. In this program, the user defines the start and end times in the fluorescence-versus-time curve for each event. The value of the fluorescence at the chosen start time t_{start}, just before fluorescence begins to rise, is considered the baseline. The end time t_{end} is chosen to be where the fluorescence after the event has returned to its lowest value. The program then determines the time of the maximum fluorescence t_{max} within this time window. The intervals (t_{start}, t_{max}) and (t_{max}, t_{end}) are defined as the rise phase and fall phase, respectively. Each of those phases is first best-fitted with a fifth-degree polynomial (for smoothing), and then a weighted average slope is calculated for each interval, upward for the rising phase and downward for the falling phase. Straight lines with those slopes are then pinned to the positions of the maximum (upward or downward) slopes of the fluorescence data and extrapolated to the baseline. The time period between the baseline intercept of the rising phase straight line and the falling phase straight line is considered to be the duration of the event. Fig. 5 A shows a schematic of this procedure and examples of the analysis.

For pTIRF experiments, two IDL programs were used to evaluate membrane curvature during secretion. Together, the programs remove background fluorescence from P- and S-polarized DiD images and create stacks of pHl, *P/S*, and *P*+2*S* images. Regions of interest are selected and values are plotted against time. The lengths of *P/S* changes were measured manually and semiquantitatively. The time that *P/S* took to return to the prefusion baseline was determined to be less than 1 s, 1–10 s, or longer than 10 s.

Online supplemental material

Supplemental Methods contains sequences of synthetic gBlocks, quantification of immunocytochemistry in transfected cells, and cartoons explaining the pTIR FM method. Fig. S1 shows that tPA has no effect on the mean PAI immunoreactivity per punctum. Fig. S2 shows coexpression of untagged tPA with PAI-pHL or NPY-pHL. Fig. S3 shows the extent of PAI overexpression: transfected vs endogenous PAI. Fig. S4 illustrates the *P/S* response after secretory granule fusion in pTIR FM. Fig. S5 illustrates the *P*+2*S* response after secretory granule fusion in pTIRF.

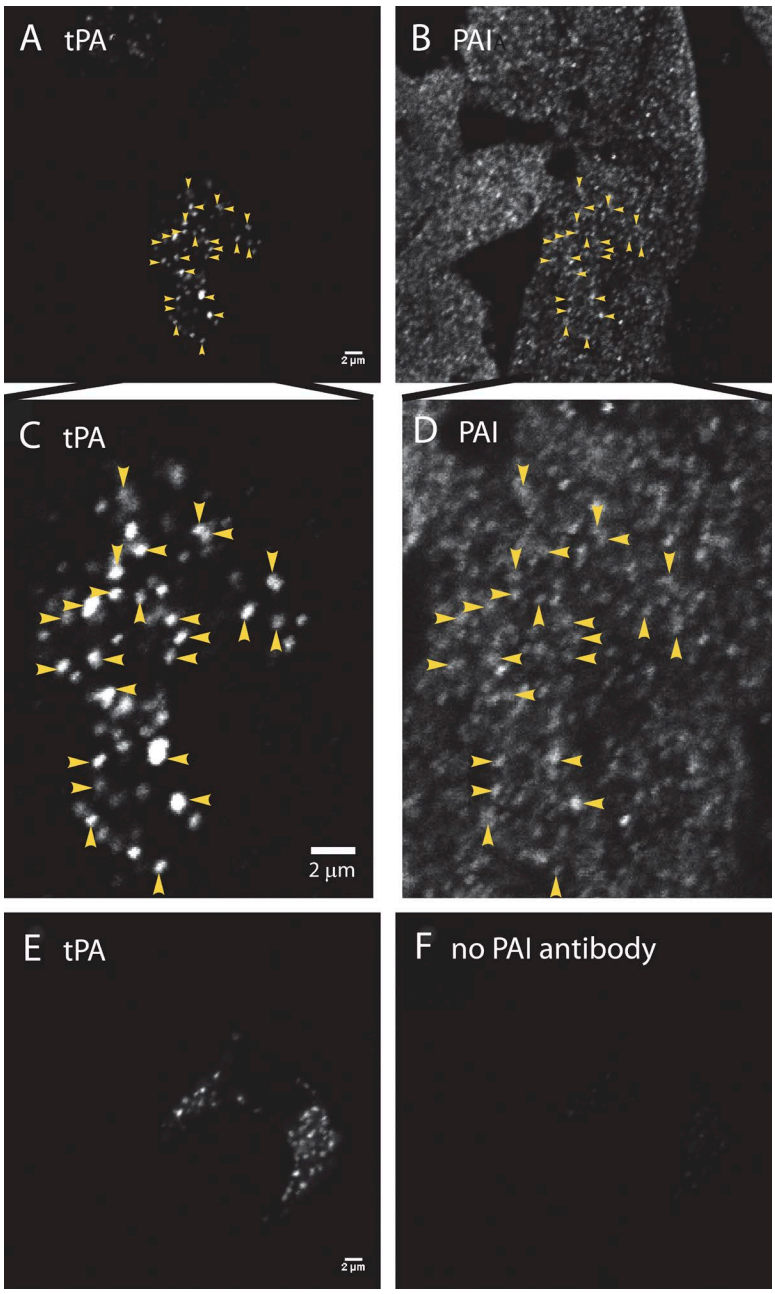

Figure 1. **PAI colocalizes with endogenous tPA in secretory granules.** (A, C, and E) Cultured bovine chromaffin cells were fixed with 4% paraformaldehyde, permeabilized with methanol, and incubated with a primary antibody to tPA (rabbit anti-mouse tPA; Molecular Innovations), followed by Alexa Fluor 488–labeled goat anti–rabbit Fab fragments (Jackson ImmunoResearch Laboratories). Fab fragments rather than bivalent antibodies were used to preclude capture of a second rabbit primary antibody in a subsequent labeling step. After rinsing, the cells were blocked with an excess of unlabeled goat anti–rabbit Fab fragments (Jackson ImmunoResearch Laboratories), to ensure that none of the first primary ab (rabbit anti-tPA) would be accessible to a second anti-rabbit secondary antibody. (B, D, and F) Cells were next incubated with (B, D) or without (F) rabbit anti–human PAI (Abcam), followed by an Alexa Fluor 546–labeled anti-rabbit secondary antibody (B, D, and F; Molecular Probes). Cells were imaged by confocal microscopy. Images to be compared directly (e.g., A and E; B and F) were acquired at the same microscope settings, and the brightness and contrast were adjusted identically in making the figures. The absence of immunofluorescence in F (with no second primary antibody against PAI) indicates that the first rabbit primary antibody visualized in E was completely blocked before the addition of the second primary (seen in B and D). Colocalization of PAI (B) and tPA (A) is indicated by arrowheads and at an expanded scale in D and C, respectively. Bars, 2 µm.

RESULTS

PAI colocalizes with endogenous tPA in secretory granules

We previously found that tPA is strongly expressed in ~20% of chromaffin cells in culture, where it has a distinct punctate appearance indicative of secretory granules (Weiss et al., 2014b). Jiang et al. (2011) used immunogold labeling and electron microscopy to detect PAI in dense core granules in PC-12 cells and isolated bovine chromaffin granules. The percentage of chromaffin cells expressing PAI was not determined.

We thus asked whether PAI was present in those chromaffin cells that express tPA, and if so, whether PAI localized to tPA-containing secretory granules or to another granule population. Cultured bovine adrenal chromaffin cells were fixed, permeabilized, and incubated with antibodies to PAI and tPA, followed by secondary antibodies conjugated with fluorescent dyes, and then imaged by confocal microscopy (Fig. 1; see Materials and methods and figure legends for details).

In contrast to immunoreactive tPA (Fig. 1, A and C), PAI immunoreactive cells were widely distributed throughout the cultures, and PAI puncta were abundant throughout the cells (Fig. 1, B and D). Not only was punctate PAI found in the subset of cells strongly expressing tPA, but PAI puncta also colocalized with tPA puncta (examples indicated by yellow arrowheads

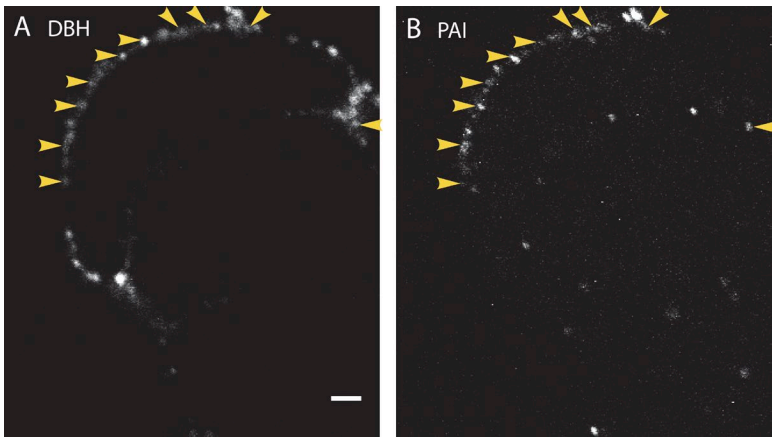

Figure 2. **Endogenous PAI colocalizes with DBH on the cell surface after stimulation.** Cultured bovine chromaffin cells were stimulated for 10 s with 56 mM K^+ at 34°C. The solution was replaced with buffer containing 5.6 mM K^+, and the cells were immediately placed on ice. Cells were then incubated with antibodies to PAI (B) and to the lumenal domain of the granule membrane protein DBH (A) for 60 min on ice, and then processed and imaged by confocal microscopy. Because the cells were not permeabilized, only antigens present on the surface of the cells are visible. Arrowheads indicate instances of colocalization of secreted DBH and PAI. n = 10 cells. Bar, 2 µm.

in Fig. 1 [C and D]). Of 788 tPA puncta analyzed in 18 cells, less than 1% (7 puncta) lacked appreciable PAI immunoreactivity, indicating that the majority of granules with endogenous tPA also contain PAI. The presence of tPA had no apparent effect on the mean PAI immunoreactivity per punctum (compare the tPA-containing cell indicated by arrowheads in Fig. 1 B to the surrounding cells without tPA). When cells with tPA (tPA fluorescence, 34,578 ± 3,867 arbitrary fluorescence units [afu]) were compared with cells without tPA (background fluorescence, 154 ± 18 afu), there was no difference in the mean PAI per punctum (30,681 ± 1,788 vs. 29,425 ± 1,880 afu, respectively; Fig. S1). We conclude that in cultured bovine cells, PAI is ubiquitously expressed in chromaffin granules, including those that contain tPA, and that the sorting of PAI to chromaffin granules is unaltered by co-storage with tPA.

Endogenous PAI colocalizes with dopamine-β-hydroxylase on the cell surface after stimulation

We and others have previously reported that components of the secretory granule membrane remain punctate on the cell surface for many seconds or minutes after fusion (Ceridono et al., 2011; Bittner et al., 2013). Chief among these is dopamine-β-hydroxylase (DBH), whose presence on the inner leaflet of the granule membrane is exposed to the extracellular space after fusion. We have also shown that certain cargo molecules (e.g., tPA-cer) may also be retained with DBH at the site of fusion for many seconds (Weiss et al., 2014a). Because PAI is in chromaffin granules, it may also be detectable on the extracellular surface at DBH-containing release sites. Intact chromaffin cells were stimulated for 10 s at 34°, immediately chilled on ice to prevent endocytosis, and incubated with antibodies to PAI and DBH. Confocal images of extracellular punctate DBH and PAI are shown in Fig. 2 (A and B), respectively. In each of 10 cells examined, PAI colocalized well with punctate DBH on the plasma membrane, consistent with PAI being released from chromaffin granules and indicating that PAI can remain associated with release sites for many seconds.

Endogenous PAI colocalizes with endogenous tPA on the cell surface after stimulation

We found that PAI and DBH colocalized at sites of granule fusion. Because endogenous PAI is co-stored with endogenous tPA in tPA-expressing cells, we asked whether the proteins also colocalize on the cell surface after fusion. Indeed, there was a striking colocalization of tPA (Fig. 3 A) and PAI (Fig. 3 B) puncta on the plasma membrane after 10-s depolarization with 56 mM K^+. In 12 cells expressing endogenous tPA, there were 333 total extracellular puncta: 30 puncta had tPA alone, 40 had PAI alone, and 263 contained both proteins. Thus, 79% of PAI and tPA puncta colocalized on the surface of stimulated cells. When the fraction of puncta with colocalized tPA and PAI was calculated for each individual cell, it ranged from 67 to 90%, with a mean of 77.2 ± 2.2%. Calculated in another manner, PAI puncta colocalized with 90% of tPA puncta on the surface of stimulated cells. As expected, neither tPA (Fig. 3 C) nor PAI (Fig. 3 D) immunoreactivity was visible on the membrane of unstimulated cells (differential interference contrast image, Fig. 3 E).

Neutralization of secretory granules allows inhibition of tPA activity

It was surprising to find that tPA, a serine protease, is routinely co-packaged and stored in the same secretory granules as its inhibitor, PAI. What prevents PAI from irreversibly inhibiting tPA before its release? One possibility is that the acidic environment of the granule (pH 5.5) prevents the inhibition of tPA by PAI. Indeed, the inhibition is strongly reduced at acid pH in vitro (Komissarov et al., 2004). If that is the case, then neutralization of the granule interior might allow the inhibition to occur. We examined whether raising the pH in intracellular chromaffin granules by incubating cells in a physiological saline solution with the weak base NH_4Cl (25 mM; Holz et al., 1983) leads to a de-

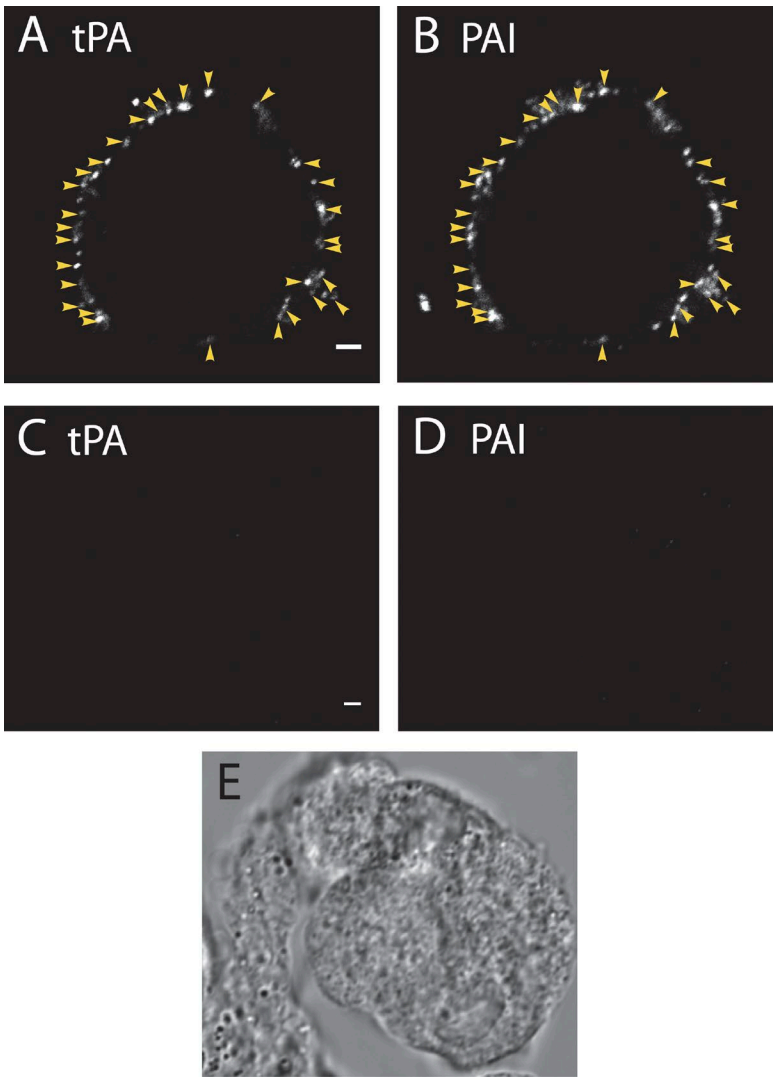

Figure 3. **Endogenous PAI colocalizes with tPA on the cell surface after stimulation.** Cultured bovine chromaffin cells were incubated for 10 s in buffer with (A and B) or without (C–E) 56 mM K^+ at 34°C. The solution was replaced with buffer containing 5.6 mM K^+, and the cells were immediately placed on ice. Cells were then incubated with antibodies to tPA (A and C) and PAI (B and D) for 60 min on ice, and then processed and imaged by confocal microscopy. (A and B) Arrowheads indicate instances of colocalization of secreted tPA and PAI. When the fraction of puncta with colocalized tPA and PAI was calculated for $n = 12$ cells, it ranged from 67 to 90%, with a mean of 77.2 ± 2.2%. $n = 333$ total puncta. (C–E) Unstimulated cells, which were processed for tPA and PAI and visualized as in A and B, have little or no secreted tPA or PAI on the plasma membrane. Images that are to be compared directly (e.g., A and C; B and D) were acquired at the same microscope settings and adjusted to the same brightness and contrast when making the figures. Bars, 2 µm.

crease in tPA activity (Fig. 4). tPA activity was measured by separating cell lysates on a gel (zymogram) polymerized in the presence of two substrates, plasminogen and casein. Active tPA cleaves the plasminogen to plasmin, which then hydrolyzes casein, leaving a clear band in a Coomassie-stained gel. In Fig. 4 A, triplicate samples (shown in inverted grayscale) were scanned and quantified (Fig. 4 B). A 90-min incubation with 25 mM NH_4Cl reduced the mean tPA activity by 47%. These findings indicate that endogenous tPA is co-stored and co-secreted with its inhibitor PAI and is protected from inactivation by the low intragranular pH.

Next we explored with transfected, labeled proteins the effects of their co-storage on the dynamics of postfusion discharge, fusion pore expansion, and the implications of the postfusion rise in pH on inactivation of tPA.

Comparison of the postfusion discharge of NPY, tPA, and PAI labeled with pHluorin

Secretory granule fusion and discharge of lumenal proteins were detected using proteins fused to the highly pH-sensitive GFP variant, ecliptic pHluorin (pHl; Miesenböck and Rothman, 1997). There was a rapid increase in fluorescence at individual fusion sites for all three proteins because of the rapid rise of pH upon fusion. However, the subsequent kinetics of the decay of fluorescence varied with the different proteins. NPY-pHl was usually discharged rapidly from the fused granule. At an acquisition rate of 36 Hz, many discharge events occurred over two to three frames (56–83 ms), and the majority of NPY events were completed in fewer than six frames (166 ms; Fig. 5 B). In contrast, the discharge of tPA-pHl was orders of magnitude slower, occurring over tens of seconds (Fig. 5 C). These results are consistent with previously reported observations with GFP or cerulean-labeled NPY and tPA (Taraska et al., 2003; Perrais et al., 2004; Tsuboi et al., 2004; Weiss et al., 2014a).

The discharge of PAI-pHl usually displayed a biphasic release pattern (Fig. 5 D), which was observed with neither NPY-pHl nor tPA-pHl. After the increase of fluorescence upon neutralization of the secretory granule lumen, there was a rapid loss of PAI-pHl fluorescence

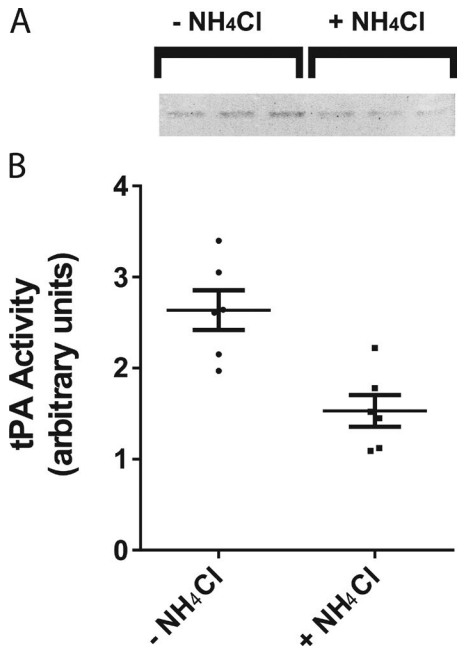

Figure 4. **Neutralization of secretory granules allows inhibition of tPA activity.** (A) Bovine chromaffin cells were incubated for 90 min in a physiological saline solution with or without 25 mM NH_4Cl at 34°C to neutralize secretory granule pH. Cell lysates were resolved on a 10% SDS polyacrylamide gel containing casein (1 mg/ml) and plasminogen (10 µg/ml). SDS was removed by four washes in 2.5% Triton X-100 to allow renaturation of tPA. Gels (zymograms) were incubated in 100 mM Tris, pH 8.1, for 4 h at 37°C and then stained with Coomassie blue stain to visualize casein hydrolysis (inverted grayscale, in triplicate). (B) Gels were scanned, and band intensities were quantified in ImageJ. Mean ± SEM is shown. Student's *t* test resulted in a p-value of 0.0027.

similar to that seen with NPY-pHl granules. However, unlike NPY-pHl or tPA-pHl, PAI-pHl fluorescence often did not smoothly decline. Instead, fluorescence rapidly decreased to approximately half of the maximal fluorescence, and then was either stable or slowly declined. The fluorescence of the plateau phase completely (and reversibly) disappeared upon perfusion with pH 5.5 buffered solution, indicating that the protein was retained on the cell surface. As shownlater (Fig. 7), the curvature changes associated with the fusion event coincide with the initial rapid phasic intensity increase and not with the plateau. Thus the plateau likely reflects the presence of PAI-pHl on the plasma membrane after the fusion pore expansion.

To quantify the duration of the postfusion discharge for the different proteins, software was developed (see Materials and Methods) that assigns a duration to individual events. The program largely eliminated subjectivity from the analysis and greatly facilitated the interpretation of the results. Examples of the analysis are shown in Fig. 5 (red and blue). In the ∼60% of the PAI-pHl events with a rapid phasic increase followed by a plateau of fluorescence, the event duration was calculated from the fluorescence changes preceding the plateau (Fig. 5 D).

The analysis confirmed that the discharge of NPY-pHl (control) was much faster than that of tPA-pHl (control), with median durations of ∼0.1 and 10 s, respectively (Fig. 6, C and E). The discharge of PAI-pHl (control) was intermediate between the other two proteins, with a median duration of ∼0.5 s (Fig. 6 A and see Fig. 9).

Expression of tPA in secretory granules slows the postfusion discharge of colocalized PAI or NPY

Immunocytochemistry (Figs. 1, 2, and 3) indicated that endogenous PAI and tPA can be packaged within the same secretory granule. tPA greatly slows the expansion of the fusion pore and, in addition, may covalently bind PAI after fusion when the granule lumen is neutralized. We therefore predicted that PAI discharge after fusion would be retarded from granules costoring tPA. Chromaffin cells were cotransfected with plasmids encoding PAI-pHl and unlabeled tPA. Immunocytochemistry revealed that ∼80% of the PAI-pHl–labeled granules coexpressed tPA (Fig. S2). There was a 1.87-fold increase in immunoreactive PAI in cells transfected with tPA-pHl and untagged PAI compared with nontransfected cells (Fig. S3). PAI-pHl cotransfected with a plasmid encoding tPA was discharged with a fivefold greater median duration than PAI-pHl cotransfected with a control plasmid (pcDNA3; Fig. 6, A and B). Coexpression of unlabeled PAI did not alter the discharge of tPA-pHl (Fig. 6, E and F).

To determine whether the ability of tPA to slow the discharge was specific for PAI-pHl, the effect of transfected tPA on the discharge of NPY-pHl was investigated. Immunocytochemistry revealed that ∼80% of the NPY-pHl–labeled granules coexpressed exogenous tPA (Fig. S2). Cotransfected tPA caused a twofold increase in the median duration of NPY-pHl events (Fig. 6, C and D). Although the effect of tPA on the discharge of NPY-pHl was less than that on the discharge of PAI-pHl, the results indicate that the ability of tPA to slow the discharge of another lumenal protein is not specific for PAI.

tPA causes a prolonged fusion pore neck in the presence of PAI and NPY

Fusion of the secretory granule membrane with the plasma membrane is accompanied by a sudden increase in the local curvature of the plasma membrane at the fusion site (Anantharam et al., 2010b, 2011). Curvature at the fusion junction can be detected by a combination of polarization and TIRF of an oriented membrane fluorophore (a carbocyanine dye, e.g., DiD), which incorporates into the plasma membrane bilayer with its preferred polarization of light absorption and emission parallel to the local plane of the membrane (Axelrod,

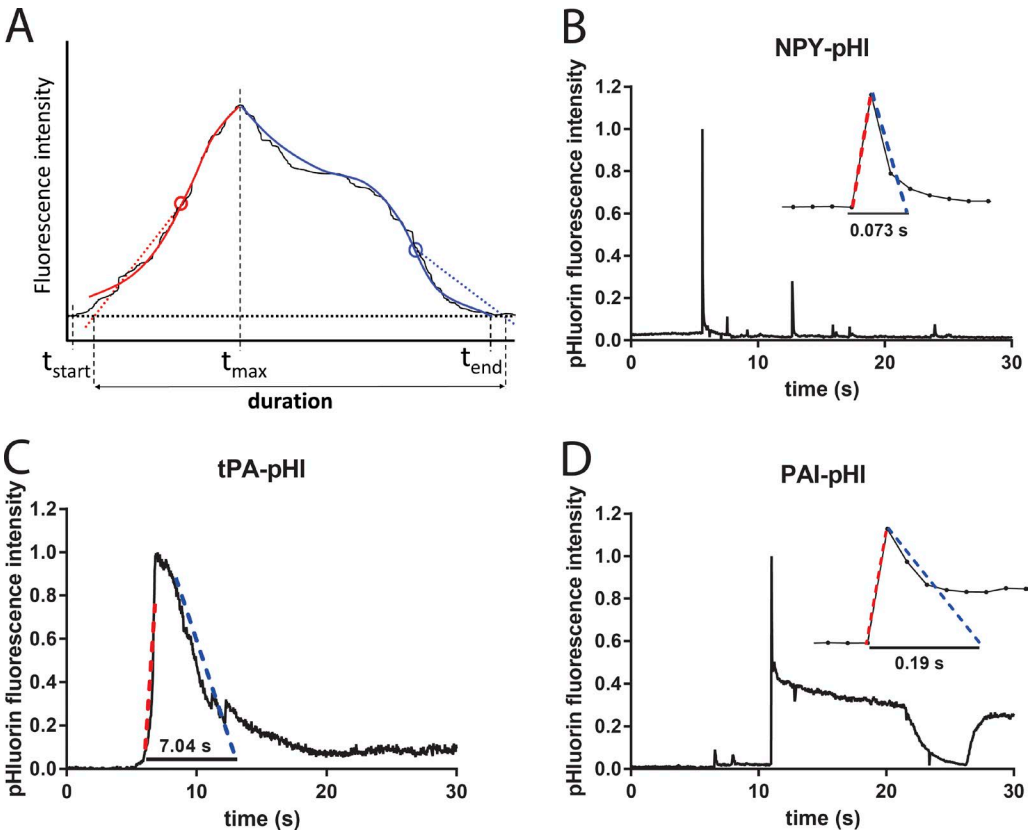

Figure 5. **NPY, tPA, and PAI have different secretion characteristics.** Bovine chromaffin cells were transfected to express cargo proteins fused to pHl. Secretion was stimulated with 56 mM potassium buffer and observed by TIRF microscopy at a rate of 36 Hz. pHl fluorescence intensity was analyzed with a custom duration-finding program that is robust against variations in the shape of the data curve. (A) Schematic of program features. The solid thin black curve is the noisy fluorescence versus time of hypothetical data. A start time t_{start} is chosen, at which the fluorescence is defined to be baseline. Analysis is done separately for the rising phase (red) and the falling phase (blue), defined as before or after the fluorescence maximum time t_{max}, respectively. First, the fluorescence versus time in each phase is smoothed by fitting to a fifth-degree polynomial (thick red or blue solid lines). Next, a weighted average slope is calculated for each phase in the respective time windows (t_{start}, t_{max}) and (t_{max}, t_{end}). Straight lines with those slopes (shown as dotted lines) are pinned to the maximum slope points (denoted by circles) and then extrapolated to the baseline to determine the event duration. (B) NPY-pHl is secreted rapidly. Entire events frequently take less than five frames at 36 Hz (inset; each point is one frame). Although the analysis was performed on a region of interest encompassing only the largest (first) fluorescent change, fluorescence changes from nearby fusion events are also evident. (C) tPA-pHl is secreted slowly, frequently lasting many seconds. (D) PAI-pHl is secreted rapidly. Often, ~50% of PAI-pHl fluorescence is immediately lost, over just a few frames (inset). A fraction of PAI-pHl remains on the cell surface (plateau) and is sensitive to a pH 5.5 solution applied extracellularly.

1979; Fig. S4). TIRF microscopy relies on the two possible orthogonal electric field polarizations of an evanescent field: one predominantly along the *z* axis (optical axis perpendicular to the coverslip, P-polarized), and the other in the plane of the coverslip (S-polarized). P-polarized light excites only membrane DiD with an absorption dipole component that is perpendicular to the coverslip, whereas S-polarized excites only DiD that has an absorption dipole component parallel to the coverslip. The key curvature measurement is an increase in the ratio of the emission with P-polarized excitation to the emission with S-polarized excitation (termed P/S). We earlier demonstrated that the curvature changes associated with the fusion of tPA-containing granules had a many-fold longer duration than those of NPY-containing granules (Weiss et al., 2014a). The slow discharge of tPA was associated with long duration curvature changes. We wanted to determine whether the prolonged fusion pore associated with fusion of a tPA-containing granule also occurred when tPA was coexpressed with PAI-pHl or NPY-pHl.

When PAI-pHl was transfected into cells without tPA, increases in membrane curvature (as determined by an increase in P/S) frequently matched the duration of the initial spike in PAI-pHl fluorescence (Fig. 7, A and B). Curvature changes and thus the fusion pore were not associated with the fluorescence plateau of the fusion event. Because the plateau was quenched by low pH, the plateau likely reflects deposition and local binding of PAI-pHl at the surface of the cell after the granule membrane flattens into the plasma membrane.

Coexpression of exogenous tPA with PAI-pHl increased the duration of the P/S elevation compared

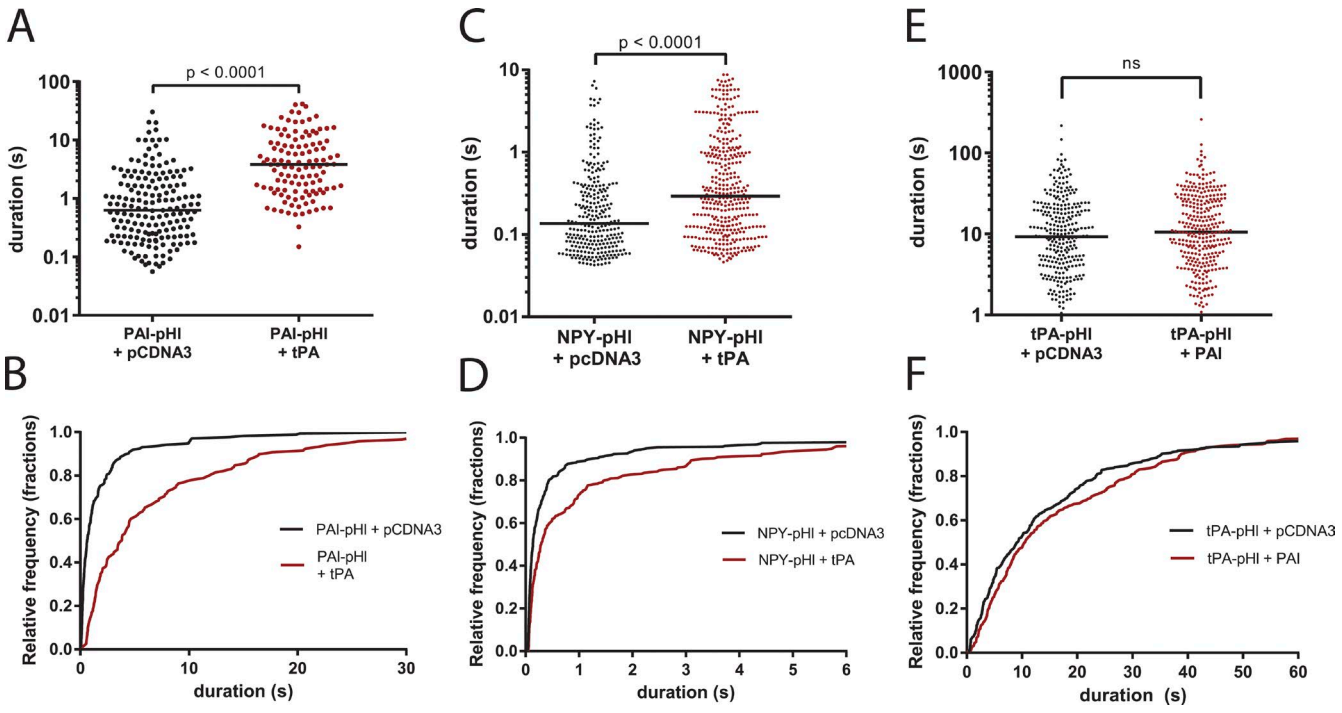

Figure 6. **tPA slows the release of co-packaged PAI-pHl and NPY-pHl.** Bovine chromaffin cells were cotransfected to express cargo proteins tagged with pHl in tandem with tPA, PAI, or pCDNA3 vector control. Secretion was stimulated with 56 mM potassium buffer and observed by TIRF microscopy at a rate of 36 Hz. pHl fluorescence intensity was analyzed with a custom program as described in Fig. 5. (A and B) tPA slows PAI-pHl secretion. (C and D) tPA slows NPY-pHl secretion. (E and F) PAI does not slow the secretion of tPA-pHl. Each dot represents one fusion event, and medians are indicated by lines. Cumulative histograms plot data from upper panels. A Kolmogorov–Smirnoff test was performed for A and C. One-way ANOVA was performed in E with a post hoc Kruskal–Wallis test.

with expression of PAI-pHl alone (Fig. 7, C and D). Coexpression increased the fraction of events that had P/S durations greater than 10 s from 25% to 76% (Fig. 7 E). tPA caused a similar increase in duration of curvature associated with the fusion pore when coexpressed with NPY-pHl (Fig. 8).

Information about the geometry of the fusion pore can be extracted from the p-TIRF measurements (Fig. S5). The linear combination of the emissions *P+2S* reports approximate total DiD emission as observed by a 1.49-NA objective, which in theory is proportional to the amount of DiD at any *x-y-z* location multiplied by the evanescent field intensity (Anantharam et al., 2010b). Computer simulations (Anantharam et al., 2010b) indicate that *P+2S* will increase if the geometry results in more DiD-labeled membrane close to the glass interface, as when a fused granule is attached to the plasma membrane by a short narrow neck. *P+2S* will decrease if DiD diffuses into a postfusion membrane indentation (placing DiD farther from the substrate and thereby in a dimmer evanescent field intensity). *P+2S* is not as robust a measurement as *P/S* because an increase, decrease, or no detectable change in *P+2S* is possible depending on various countervailing tendencies arising from the geometrical details of the membrane deformation. In those fusion events of granules containing tPA alone or tPA with either PAI-pHl or NPY-pHl with measurable change in *P+2S*, ~90% had an increase in *P+2S*. Thus, it is likely that tPA with or without colocalization with other transfected proteins in secretory granules preferentially stabilizes a geometry that occurs soon after fusion, with the granule membrane connected to the plasma membrane through a short narrow neck.

Mutation of the active-site serine in tPA does not alter the retarded release of coexpressed PAI-pHl

We investigated whether the ability of tPA to slow the release of co-stored PAI is caused not only by delayed fusion pore expansion, but also by the covalent attachment of PAI to tPA at the active site serine (serine 513). This reaction is likely to occur upon the increase of lumenal pH after fusion but before complete discharge of PAI. The possibility was investigated by cotransfecting PAI-pHL with either wild-type tPA or tPA (S513A; Fig. 9). The median discharge duration was increased from 0.4 s in the absence of transfected tPA to 14 s by both wild-type and mutant tPA. Both wild-type and mutant tPA slowed PAI-pHl discharge similarly. Thus, the covalent interaction of PAI with tPA does not contribute to the effect of tPA to slow PAI discharge after fusion.

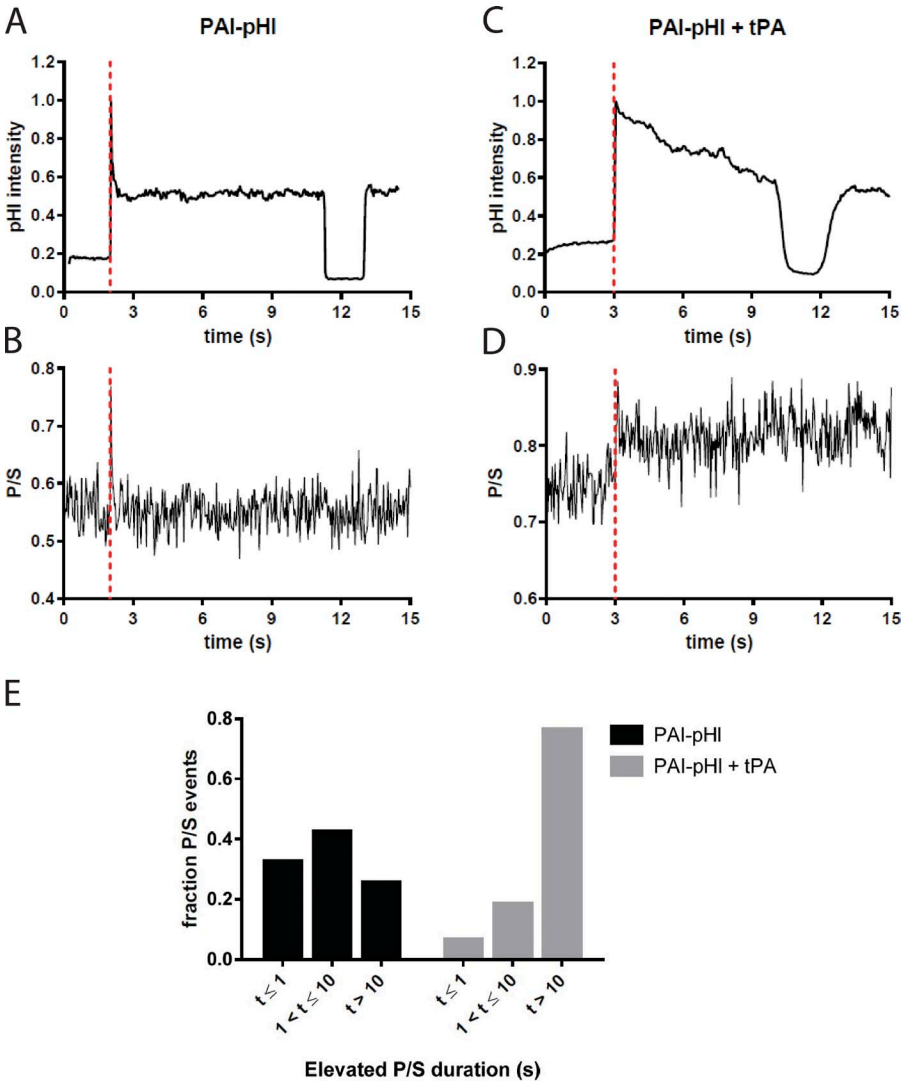

Figure 7. **tPA slows fusion pore expansion in the presence of PAI-pHl.** Bovine chromaffin cells were cotransfected with either PAI-pHl and pcDNA3 or PAI-pHl and tPA. pTIRF microscopy was performed as described in Materials and Methods. (A and C) Changes in pHluorin fluorescence were recorded over time. (B and D) Concurrently, DiD fluorescence as excited by P- and S-polarized light was recorded. The ratio *P/S*, plotted against time, corresponds to localized increases in membrane curvature. Secretion start time is indicated by the dotted red line. (E) Increases in *P/S* are reported semiquantitatively. The length of time *P/S* was elevated was measured for $n = 40$ PAI-pHl + pcDNA3 or $n = 17$ PAI-pHl = tPA events and binned as shown.

DISCUSSION

We previously reported that a lumenal cargo protein within a secretory granule strongly inhibits the expansion of its own fusion pore, thereby slowing its own postfusion discharge. tPA is endogenously expressed in a subpopulation of chromaffin cells and had been implicated in an autocrine/paracrine negative feedback pathway that is initiated by proteolytic activation of surface plasminogen to plasmin. By regulation of its own discharge, tPA is likely shaping the kinetics of the extracellular proteolytic pathway. Here we describe another consequence of the regulation of the fusion pore. The fused granule with a stable fusion pore causes the high concentrations of retained proteins within the granule lumen to be suddenly exposed to neutral pH. In this context, we considered the finding that tPA and its primary protein inhibitor, PAI, are both expressed in chromaffin cells and both are secreted upon stimulation (Parmer et al., 1997; Jiang et al., 2011).

Endogenous PAI and tPA are co-packaged in the same secretory granules in chromaffin cells and can be detected on the cell surface

PAI is a suicide substrate that irreversibly acylates the active site in tPA at neutral pH (Lawrence et al., 1995). Previous studies demonstrated by sucrose density purification that both tPA and PAI are localized in chromaffin granules (Parmer et al., 1997; Jiang et al., 2011). In the present study, we used immunocytochemistry to examine the localization of the endogenous proteins in chromaffin cells. PAI was expressed in the majority of chromaffin cells in the cultures as small puncta, strongly suggesting that they were in chromaffin granules. Indeed, upon brief stimulation (10 s) with elevated K^+, PAI that had not yet diffused into the medium was found on the cell surface in small puncta also containing membrane-bound DBH, a lumenal marker of chromaffin granules. Whereas PAI was expressed in most of the chromaffin cells, tPA is expressed in only 20% (Weiss et al., 2014b). Remarkably, tPA expression in chromaffin granules was invariably associated with

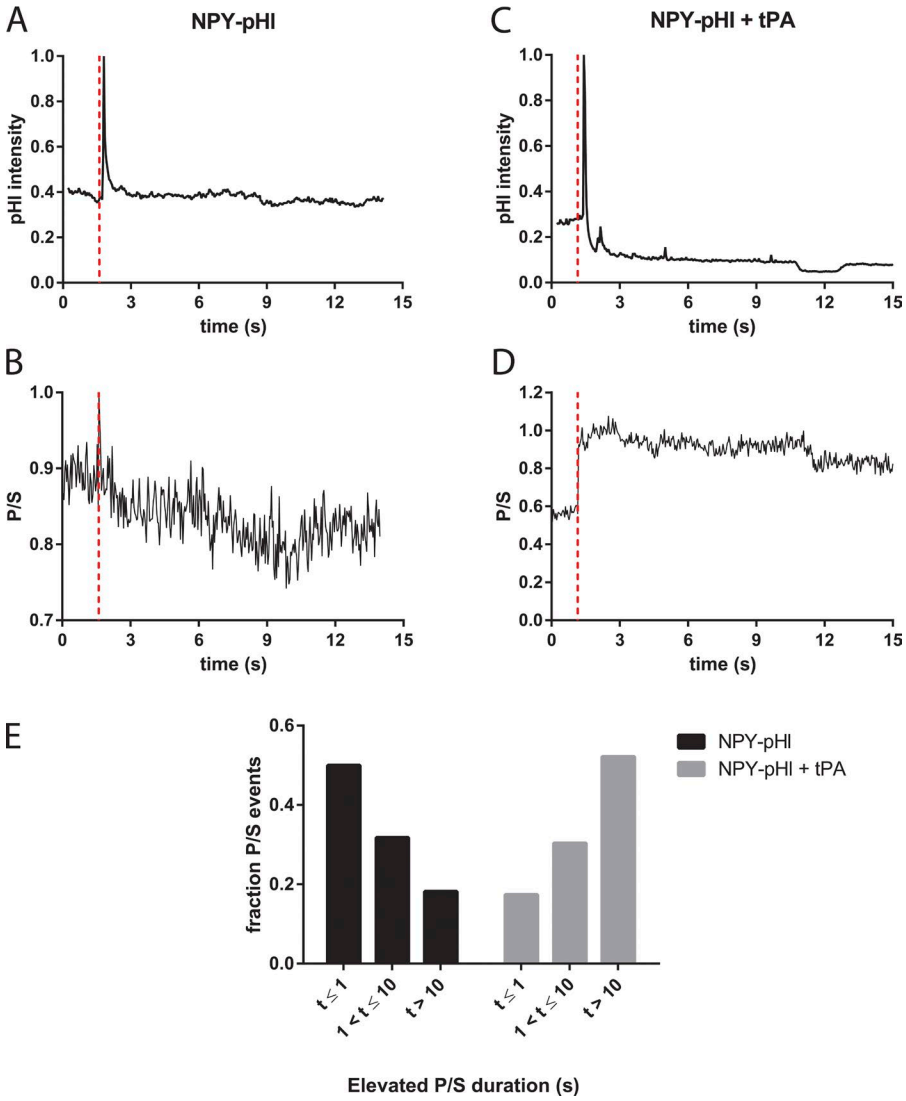

Figure 8. **tPA slows fusion pore expansion in the presence of NPY-pHl.** Bovine chromaffin cells were cotransfected with either NPY-pHl and pcDNA3 or NPY-pHl and tPA. pTIRF microscopy was performed as described in Materials and Methods. (A and C) Changes in pHl fluorescence were recorded over time. (B and D) Concurrently, DiD fluorescence as excited by P- and S-polarized light was recorded. The ratio *P/S*, plotted against time, corresponds to localized increases in membrane curvature. Secretion start time is indicated by the dotted red line. (E) Increases in *P/S* are reported semi-quantitatively. The length of time *P/S* was elevated was measured for $n = 22$ NPY-pHl + pcDNA3 or $n = 33$ NPY-pHl = tPA events and binned as shown.

coexpression of its inhibitor PAI (Fig. 1). In a previous study, we demonstrated that endogenous tPA, like PAI, appears on the cell surface as puncta colocalized with DBH after a 10-s stimulation (Weiss et al., 2014a). Not surprisingly, when cells were stimulated with elevated K^+, endogenous tPA was colocalized with endogenous PAI on the cell surface in puncta (Fig. 3), indicative of co-discharge of the co-packaged proteins.

We reckoned that the low pH of chromaffin granules (pH 5.3–5.5; Holz et al., 1983) protects tPA from inactivation. Indeed, when the lumenal pH of intracellular chromaffin granules was raised by incubation of cells with NH_4Cl, subsequent zymography of cell homogenates demonstrated that tPA activity was inhibited 50% (Fig. 4). Because the covalent interaction of tPA and PAI is robust at neutral pH, these experiments indicate that endogenous tPA is protected from covalent inhibition by PAI because of the low lumenal pH, but can be rapidly inactivated upon the rise of intralumenal pH with fusion. Thus, the punctate tPA that colocalizes with PAI on the cell surface immediately upon fusion is likely to be at least partially inhibited.

tPA creates a nanoscale chamber upon fusion that permits covalent interaction with PAI

The colocalization of endogenous PAI with tPA prompted us to investigate the effect of tPA on the discharge of co-stored fluorescently labeled PAI. PAI-pHl discharge in the absence of transfected tPA often had an unusual time course. There was rapid partial release (within 1–2 s) followed by stable fluorescence for tens of seconds on the extracellular surface (Fig. 5 D). Because pTIRF microscopy detected curvature only during the initial rapid release, it is likely that the retained fluorescence reflects PAI-pHl binding to the cell surface after expansion of the fusion pore.

Co-storage with transfected tPA slowed the initial discharge of PAI-pHl at least fivefold (Fig. 6). Because the discharge of NPY-pHl was also slowed by co-storage with tPA, at least part of the retention of PAI-pHl by tPA was

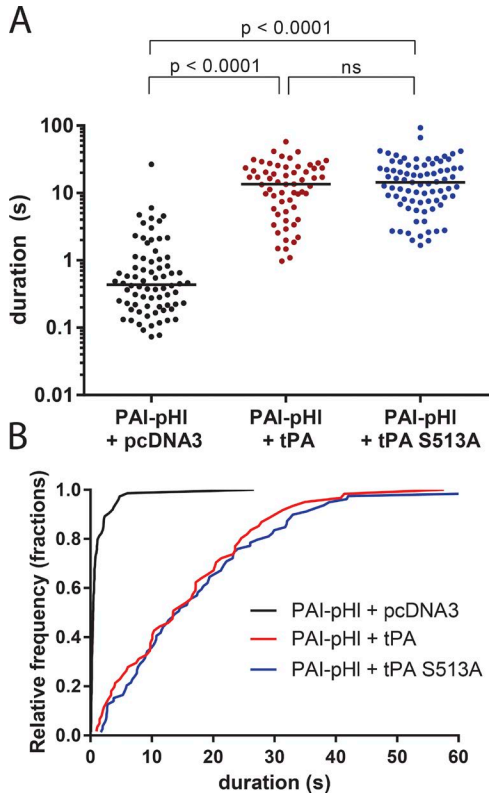

Figure 9. **A kinase-dead mutant of tPA still slows PAI-pHl secretion.** Bovine chromaffin cells were cotransfected to express PAI-pHl in tandem with tPA, S513A tPA, or empty vector control (pcDNA3). Secretion was stimulated with 56 mM potassium buffer and observed by TIRF microscopy at a rate of 36 Hz. pHl fluorescence intensity was analyzed with a custom program as described in Fig. 5. (A) Each dot represents one fusion event. Medians are indicated by lines. One-way ANOVA was performed with a post hoc Kruskal–Wallis test. (B) Cumulative histogram plots data from A.

likely caused by the profound slowing of fusion pore expansion induced by tPA (detected by pTIRF; Fig. 7). Indeed, the ability of tPA to slow fusion pore expansion can even retard the discharge of catecholamine detected by amperometry (Weiss et al., 2014a).

Binding of PAI-pHl to the slowly discharged tPA may also contribute to the retardation of PAI-pHl discharge. We showed with tPA having its active site serine mutated to alanine that the slowing of PAI discharge did not require covalent interaction of PAI and tPA (Fig. 9). However, because PAI binds to tPA even without acylation (Olson et al., 2001), noncovalent interaction with tPA could contribute to the slow discharge kinetics.

Function of a nanoscale reaction chamber

There are at least two possible consequences of the formation of a nanoscale reaction chamber. First, the amount of enzymatically active tPA that is discharged is likely to be lessened because of inhibition by co-stored PAI immediately upon the neutralization of the granule interior upon fusion. Zymography indicated that 50% of the tPA activity was retained after the pH within intracellular secretory granules was raised by incubation with NH_4^+, suggesting that there is a molar excess of endogenous tPA over PAI in secretory granules. This finding is consistent with enzymatically active tPA being secreted from chromaffin cells upon stimulation (Parmer et al., 1997).

Is there enough time between the rise in lumenal pH upon fusion and discharge of PAI to permit the covalent inactivation of tPA by PAI? The reaction should be complete within a millisecond of pH neutralization, based on the rate constant of the interaction of the two proteins in vitro (Lawrence et al., 1990) and assuming that the endogenous proteins are as little as 1% by weight (~30–70 µM concentrations) of the total lumenal granule protein (~250 mg/ml; R.W. Holz, personal observations). If these concentrations of free proteins are actually present in the granule, then little unreacted PAI would be discharged, because the discharge time for total PAI-pHl is greater than 1 s for 90% of the fusions in the presence of tPA (Fig. 6, A and B). However, there is great uncertainty in this estimate, and the reaction rates could be orders of magnitude slower. The free concentrations of endogenous tPA and PAI are unknown. Indeed, tPA can be quite insoluble at neutral or acid pH (~0.1 mg/ml; Nguyen and Ward, 1993). In addition, because the kinetics were determined in dilute and ideal reaction conditions, the reaction rate may be much less in the unusual environment of the recently fused granule. Therefore, we cannot rule out the possibility that some unreacted PAI and tPA escapes through the slowly expanding fusion pore, and thus reduces the amount of the tPA/PAI complex. Nevertheless, there seems to be more than enough time to allow the inhibition of tPA and the creation of a new secreted species.

A second consequence of the formation of a nanoscale reaction chamber after fusion is the formation of the covalent tPA/PAI complex. The complex may have physiological function. It is a high affinity ligand for the LDL receptor-related protein (LRP-1); binding to LRP-1 results in its endocytosis (Stefansson et al., 1998; Lillis et al., 2005). LRP-1 also functions as an intracellular scaffold for protein kinase signaling pathways (Lillis et al., 2005; Mantuano et al., 2013). The signaling effects of binding tPA/PAI are unknown. Because LRP-1 mRNA is expressed in human adrenal medulla (Uhlén et al., 2015), the locally released tPA/PAI complex may itself have autocrine/paracrine affects. Secreted tPA/PAI complexes may also have systemic effects mediated through interaction with LRP-1 at distal sites (Cale and Lawrence, 2007).

In summary, our results, as well those of Chiang et al. (2014), highlight the fact that omega-figure–like structures can have durations of many seconds after fusion. The present study proposes that these structures

can have important physiological consequences. The slow postfusion discharge of tPA has been observed by numerous investigators in different cells (Taraska et al., 2003; Perrais et al., 2004; Tsuboi et al., 2004) including vascular endothelial cells (Suzuki et al., 2009). The present study places these observations in a new context. We reveal the surprising discovery that PAI, the physiological inhibitor of tPA, is coexpressed in secretory granules and co-discharged with tPA. We demonstrate with pTIRFM that tPA slows its own fusion pore expansion in the presence (and absence) of PAI, thereby slowing discharge of lumenal contents and creating a neutral pH nanoscale reaction chamber on the cell surface. This chamber permits the covalent interaction of inhibitor and enzyme, and thereby creates a new secreted product with potential intra- and intercellular signaling function.

ACKNOWLEDGMENTS

We are grateful to Mark Warnock for providing expert advice about zymography and antibodies standards for tPA and PAI. We thank Dr. Prabhodh Abbineni for helpful discussions about this work and experimental assistance.

This work was supported by National Institutes of Health grants R01-170553 to R.W. Holz and D. Axelrod, R01 HL55374 to D.A. Lawrence, and T32-HL-007853 to K.P. Bohannon.

The authors declare no competing financial interests.

Author contributions: K.P. Bohannon conceived, performed, and analyzed experiments and was a major contributor to the writing of the paper. M.A. Bittner conceived, performed, and analyzed experiments and was a major contributor to the writing of the paper. D.A. Lawrence helped design experiments. D. Axelrod developed mathematical methods for analyzing secretion events and contributed to the writing of the paper. R.W. Holz helped conceive of the experiments and contributed significantly to the writing of the paper.

Sharona E. Gordon served as editor.

Submitted: 27 June 2017
Accepted: 21 August 2017

REFERENCES

Anantharam, A., D. Axelrod, and R.W. Holz. 2010a. Polarized TIR FM reveals changes in plasma membrane topology before and during granule fusion. *Cell. Mol. Neurobiol.* 30:1343–1349. http://dx.doi.org/10.1007/s10571-010-9590-0

Anantharam, A., B. Onoa, R.H. Edwards, R.W. Holz, and D. Axelrod. 2010b. Localized topological changes of the plasma membrane upon exocytosis visualized by polarized TIRFM. *J. Cell Biol.* 188:415–428. http://dx.doi.org/10.1083/jcb.200908010

Anantharam, A., M.A. Bittner, R.L. Aikman, E.L. Stuenkel, S.L. Schmid, D. Axelrod, and R.W. Holz. 2011. A new role for the dynamin GTPase In the regulation of fusion pore expansion. *Mol. Biol. Cell.* 22:1907–1918. http://dx.doi.org/10.1091/mbc.E11-02-0101

Axelrod, D. 1979. Carbocyanine dye orientation in red cell membrane studied by microscopic fluorescence polarization. *Biophys. J.* 26:557–573. http://dx.doi.org/10.1016/S0006-3495(79)85271-6

Bittner, M.A., R.L. Aikman, and R.W. Holz. 2013. A nibbling mechanism for clathrin-mediated retrieval of secretory granule membrane after exocytosis. *J. Biol. Chem.* 288:9177–9188. http://dx.doi.org/10.1074/jbc.M113.450361

Brees, C., and M. Fransen. 2014. A cost-effective approach to microporate mammalian cells with the neon transfection system. *Anal. Biochem.* 466:49–50. http://dx.doi.org/10.1016/j.ab.2014.08.017

Cale, J.M., and D.A. Lawrence. 2007. Structure-function relationships of plasminogen activator inhibitor-1 and its potential as a therapeutic agent. *Curr. Drug Targets.* 8:971–981. http://dx.doi.org/10.2174/138945007781662337

Ceridono, M., S. Ory, F. Momboisse, S. Chasserot-Golaz, S. Houy, V. Calco, A.M. Haeberle, V. Demais, Y. Bailly, M.F. Bader, and S. Gasman. 2011. Selective recapture of secretory granule components after full collapse exocytosis in neuroendocrine chromaffin cells. *Traffic.* 12:72–88. http://dx.doi.org/10.1111/j.1600-0854.2010.01125.x

Chiang, H.C., W. Shin, W.D. Zhao, E. Hamid, J. Sheng, M. Baydyuk, P.J. Wen, A. Jin, F. Momboisse, and L.G. Wu. 2014. Post-fusion structural changes and their roles in exocytosis and endocytosis of dense-core vesicles. *Nat. Commun.* 5:3356. http://dx.doi.org/10.1038/ncomms4356

Dietrich, K., G.D. Ball, and L.G. Mitchell. 2016. Increased plasminogen activator inhibitor results in a hypofibrinolytic state in adolescents with obesity: In vivo and ex vivo evidence. *Br. J. Haematol.* 175:300–307. http://dx.doi.org/10.1111/bjh.14238

Fugate, J.E., and A.A. Rabinstein. 2014. Update on intravenous recombinant tissue plasminogen activator for acute ischemic stroke. *Mayo Clin. Proc.* 89:960–972. http://dx.doi.org/10.1016/j.mayocp.2014.03.001

Holz, R.W., R.A. Senter, and R.R. Sharp. 1983. Evidence that the H + electrochemical gradient across membranes of chromaffin granules is not involved in exocytosis. *J. Biol. Chem.* 258:7506–7513.

Jiang, Q., N.A. Gingles, M.A. Olivier, L.A. Miles, and R.J. Parmer. 2011. The anti-fibrinolytic SERPIN, plasminogen activator inhibitor 1 (PAI-1), is targeted to and released from catecholamine storage vesicles. *Blood.* 117:7155–7163. http://dx.doi.org/10.1182/blood-2010-05-287672

Komissarov, A.A., P.J. Declerck, and J.D. Shore. 2004. Protonation state of a single histidine residue contributes significantly to the kinetics of the reaction of plasminogen activator inhibitor-1 with tissue-type plasminogen activator. *J. Biol. Chem.* 279:23007–23013. http://dx.doi.org/10.1074/jbc.M401383200

Ladenvall, P., U. Wall, S. Jern, and C. Jern. 2000. Identification of eight novel single-nucleotide polymorphisms at human tissue-type plasminogen activator (t-PA) locus: Association with vascular t-PA release in vivo. *Thromb. Haemost.* 84:150–155.

Lawrence, D.A., L. Strandberg, J. Ericson, and T. Ny. 1990. Structure-function studies of the SERPIN plasminogen activator inhibitor type 1. Analysis of chimeric strained loop mutants. *J. Biol. Chem.* 265:20293–20301.

Lawrence, D.A., D. Ginsburg, D.E. Day, M.B. Berkenpas, I.M. Verhamme, J.O. Kvassman, and J.D. Shore. 1995. Serpin-protease complexes are trapped as stable acyl-enzyme intermediates. *J. Biol. Chem.* 270:25309–25312. http://dx.doi.org/10.1074/jbc.270.43.25309

Lillis, A.P., I. Mikhailenko, and D.K. Strickland. 2005. Beyond endocytosis: LRP function in cell migration, proliferation and vascular permeability. *J. Thromb. Haemost.* 3:1884–1893. http://dx.doi.org/10.1111/j.1538-7836.2005.01371.x

Loscalzo, J., and E. Braunwald. 1988. Tissue plasminogen activator. *N. Engl. J. Med.* 319:925–931. http://dx.doi.org/10.1056/NEJM198810063191407

Mantuano, E., M.S. Lam, and S.L. Gonias. 2013. LRP1 assembles unique co-receptor systems to initiate cell signaling in response to tissue-type plasminogen activator and myelin-associated

glycoprotein. *J. Biol. Chem.* 288:34009–34018. http://dx.doi.org/10.1074/jbc.M113.509133

Miesenböck, G., and J.E. Rothman. 1997. Patterns of synaptic activity in neural networks recorded by light emission from synaptolucins. *Proc. Natl. Acad. Sci. USA.* 94:3402–3407. http://dx.doi.org/10.1073/pnas.94.7.3402

Miyata, S., Y. Nakatani, N. Hayashi, and T. Nakashima. 2005. Matrix-degrading enzymes tissue plasminogen activator and matrix metalloprotease-3 in the hypothalamo-neurohypophysial system. *Brain Res.* 1058:1–9. http://dx.doi.org/10.1016/j.brainres.2005.07.027

Nguyen, T.H., and C. Ward. 1993. Stability characterization and formulation development of alteplase, a recombinant tissue plasminogen activator. *Pharm. Biotechnol.* 5:91–134. http://dx.doi.org/10.1007/978-1-4899-1236-7_3

Olson, S.T., R. Swanson, D. Day, I. Verhamme, J. Kvassman, and J.D. Shore. 2001. Resolution of Michaelis complex, acylation, and conformational change steps in the reactions of the serpin, plasminogen activator inhibitor-1, with tissue plasminogen activator and trypsin. *Biochemistry.* 40:11742–11756. http://dx.doi.org/10.1021/bi0107290

Parmer, R.J., M. Mahata, S. Mahata, M.T. Sebald, D.T. O'Connor, and L.A. Miles. 1997. Tissue plasminogen activator (t-PA) is targeted to the regulated secretory pathway. Catecholamine storage vesicles as a reservoir for the rapid release of t-PA. *J. Biol. Chem.* 272:1976–1982. http://dx.doi.org/10.1074/jbc.272.3.1976

Parmer, R.J., M. Mahata, Y. Gong, S.K. Mahata, Q. Jiang, D.T. O'Connor, X.P. Xi, and L.A. Miles. 2000. Processing of chromogranin A by plasmin provides a novel mechanism for regulating catecholamine secretion. *J. Clin. Invest.* 106:907–915. http://dx.doi.org/10.1172/JCI7394

Perrais, D., I.C. Kleppe, J.W. Taraska, and W. Almers. 2004. Recapture after exocytosis causes differential retention of protein in granules of bovine chromaffin cells. *J. Physiol.* 560:413–428. http://dx.doi.org/10.1113/jphysiol.2004.064410

Salles, F.J., and S. Strickland. 2002. Localization and regulation of the tissue plasminogen activator-plasmin system in the hippocampus. *J. Neurosci.* 22:2125–2134.

Sartori, M.T., G. Saggiorato, L. Spiezia, C. Varvarikis, G. Carraro, G.M. Patrassi, and A. Girolami. 2003. Influence of the Alu-repeat I/D polymorphism in t-PA gene intron 8 on the stimulated t-PA release after venous occlusion. *Clin. Appl. Thromb. Hemost.* 9:63–69. http://dx.doi.org/10.1177/107602960300900109

Schneider, C.A., W.S. Rasband, and K.W. Eliceiri. 2012. NIH Image to ImageJ: 25 years of image analysis. *Nat. Methods.* 9:671–675. http://dx.doi.org/10.1038/nmeth.2089

Stefansson, S., S. Muhammad, X.F. Cheng, F.D. Battey, D.K. Strickland, and D.A. Lawrence. 1998. Plasminogen activator inhibitor-1 contains a cryptic high affinity binding site for the low density lipoprotein receptor-related protein. *J. Biol. Chem.* 273:6358–6366. http://dx.doi.org/10.1074/jbc.273.11.6358

Suzuki, Y., H. Mogami, H. Ihara, and T. Urano. 2009. Unique secretory dynamics of tissue plasminogen activator and its modulation by plasminogen activator inhibitor-1 in vascular endothelial cells. *Blood.* 113:470–478. http://dx.doi.org/10.1182/blood-2008-03-144279

Taraska, J.W., D. Perrais, M. Ohara-Imaizumi, S. Nagamatsu, and W. Almers. 2003. Secretory granules are recaptured largely intact after stimulated exocytosis in cultured endocrine cells. *Proc. Natl. Acad. Sci. USA.* 100:2070–2075. http://dx.doi.org/10.1073/pnas.0337526100

Tsuboi, T., H.T. Mcmahon, and G.A. Rutter. 2004. Mechanisms of dense core vesicle recapture following "kiss and run" ("cavicapture") exocytosis in insulin-secreting cells. *J. Biol. Chem.* 279:47115–47124. http://dx.doi.org/10.1074/jbc.M408179200

Uhlén, M., L. Fagerberg, B.M. Hallstrom, C. Lindskog, P. Oksvold, A. Mardinoglu, A. Sivertsson, C. Kampf, E. Sjostedt, A. Asplund, et al. 2015. Proteomics. Tissue-based map of the human proteome. *Science.* 347:1260419. http://dx.doi.org/10.1126/science.1260419

Weiss, A.N., A. Anantharam, M.A. Bittner, D. Axelrod, and R.W. Holz. 2014a. Lumenal protein within secretory granules affects fusion pore expansion. *Biophys. J.* 107:26–33. http://dx.doi.org/10.1016/j.bpj.2014.04.064

Weiss, A.N., M.A. Bittner, R.W. Holz, and D. Axelrod. 2014b. Protein mobility within secretory granules. *Biophys. J.* 107:16–25. http://dx.doi.org/10.1016/j.bpj.2014.04.063

Wick, P.F., R.A. Senter, L.A. Parsels, and R.W. Holz. 1993. Transient transfection studies of secretion in bovine chromaffin cells and PC12 cells: Generation of kainate-sensitive chromaffin cells. *J. Biol. Chem.* 268:10983–10989.